Making a Reconfigurable Artificial Crystal by Ordering Bistable Magnetic Nanowires

Jesco Topp,[1] Detlef Heitmann,[1] Mikhail P. Kostylev,[2] and Dirk Grundler[3,*]

[1]*Institut für Angewandte Physik und Mikrostrukturforschungszentrum, Universität Hamburg,
Jungiusstrasse 11, D-20355 Hamburg, Germany*
[2]*School of Physics, M013, University of Western Australia, 35 Stirling Hwy, 6009 Crawley, Western Australia, Australia*
[3]*Lehrstuhl für Physik funktionaler Schichtsysteme, Physik Department E10, Technische Universität München,
James-Franck-Strasse, D-85747 Garching, Germany*

Spin-wave excitations (magnons) are investigated in a one-dimensional (1D) magnonic crystal fabricated out of $Ni_{80}Fe_{20}$ nanowires. We find two different magnon band structures depending on the magnetic ordering of neighboring wires, i.e., parallel and antiparallel alignment. At a zero in-plane magnetic field H the modes of the antiparallel case are close to those obtained by zone folding of the spin-wave dispersions of the parallel case. This is no longer true for nonzero H which opens a forbidden frequency gap at the Brillouin zone boundary. The 1D stop band gap scales with the external field, which generates a periodic potential for Bragg reflection of the magnons.

In solid state physics, artificial crystal (AC) effects have been realized based on different wave phenomena such as electron- [1], phonon- [2], plasmon- [3], and photonlike [4] waves. Periodic nanopatterning of metallic and dielectric materials has led to tailored wave dispersions consisting of allowed bands and forbidden frequency gaps in certain propagation directions. The reciprocal lattice constant $G = 2\pi/R$ induces the zone folding of previously monotonic dispersions $f(k)$ into the first Brillouin zone (BZ), where R is the magnitude of the primitive vector of the periodic lattice, f is the frequency, and k is the magnitude of the wave vector. Gaps occur at BZ boundaries $k = \pi/R$. ACs based on magnons, i.e., spin waves, propagating in laterally patterned ferromagnets are currently of particular interest. Pioneering experiments on nanowires magnetized all in parallel have recently evidenced the realization of a lateral magnonic crystal (MC) in one dimension (1D). Artificially tailored magnon dispersions have indeed been found [5–7]. Importantly, magnetic ACs offer specific properties that go beyond the ones known from previous nonmagnetic ACs.

In this Letter, we report on a 1D AC fabricated from nanopatterned ferromagnetic wires [Figs. 1(a) and 1(b)], where we generate different AC dispersions and forbidden frequency gaps Δ in one and the same sample. We show experimentally and theoretically how we control R externally by the magnetic nonvolatility. When the magnetization **M** of neighboring wires is antiparallel, we vary the allowed bands and Δ with an in-plane magnetic field H without significantly changing the center of the stop band. The findings offer interesting perspectives in magnonics, e.g., for tunable spin wave filters [8–12].

We have prepared a 1D magnonic crystal from an array of 20 nm-thick Permalloy ($Ni_{80}Fe_{20}$, Py) nanowires which are dipolarly coupled such as those discussed in Ref. [13] and show a bistable magnetization configuration [14,15].

The wires are all 180 μm long and 300 nm wide. The structure period is $a = 400$ nm. We have checked the dipolar coupling in that we have studied different arrays of nominally identical nanowires with edge-to-edge separations d varying between 100 and 1000 nm. Coupling has been found to be relevant for $d \leq 400$ nm (cf. Figs. 6 and 7 in Ref. [14]). We record magnetic field-dependent magnon
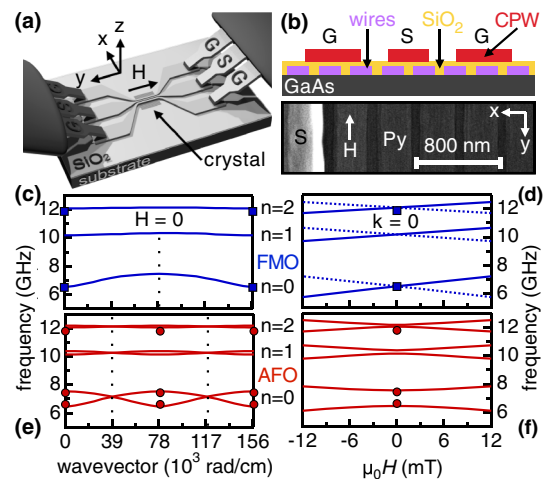

FIG. 1 (color online). (a) Sketch of the CPW with an integrated array connected to the VNA by microwave probes. The CPW consists of ground-signal-ground lines. (b) Cross section of the sample (top), not to scale. Microscopy image (bottom) of nanowires with $a = 400$ nm. (c) Calculated dispersion $f(k)$ at $H = 0$ and (d) $f(H)$ at $k = 0$ when all nanowires are magnetized in parallel. (e) Calculated dispersion $f(k)$ at $H = 0$ and (f) $f(H)$ at $k = 0$ when neighboring nanowires are magnetized antiparallel. At $k = 0$ a field-dependent mode repulsion occurs around $H = 0$. Vertical lines show BZ boundaries. We consider $l_c = 2.4$ μm and a saturation magnetization $\mu_0 M_s = 0.99$ T. Symbols are experimental data. n labels the modes. We show $f(k)$ in repeated zone schemes.

spectra using a vector-network analyzer (VNA) based spectroscopy experiment [16–19]. The VNA is connected to a coplanar waveguide (CPW) prepared on top of the magnonic crystal and oriented parallel to the nanowires [Fig. 1(a)]. A microwave current generated by the VNA excites precessional motion of spins in the wires, which results in a modified transmission $T(f)$ of the CPW [Fig. 1(b)]. By subtracting $T(f)$ obtained at the reference field $\mu_0|\mathbf{H}| = 90$ mT oriented perpendicular to the CPW, we obtain data sets $\Delta T(f)$ where magnon-induced changes of $T(f)$ exhibit a large signal-to-noise ratio [16]. The magnetic radio-frequency (rf) field $\mathbf{h}$ of the CPW is uniform above the inner conductor, which is 10 μm wide, but nonuniform in the gap between inner and outer conductors (see, Ref. [16], for example). The nonuniformity provokes a finite wave vector $k_x = 1300$ rad/cm [20]. This value is small, and magnons excited in the experiment therefore lie at the center of the BZ. We obtain theoretical spin wave dispersions through numerical calculations based on previously published approaches [13,21] and take into account, in particular, the Bloch theorem $m_{x(z)}(x) = m'_{x(z)} \exp(ik_x x)$. Here, $m'_{x(z)}(x + pR) = m'_{x(z)}(x)$ holds for the dynamic magnetization components m_x and m_z of a spin wave propagating in x direction (p is a positive or negative integer). In Figs. 1(c) and 1(e) dispersions are shown for the nanowire array from Fig. 1(b) in the two different states where neighboring wires exhibit ferromagnetic order (FMO) and antiferromagnetic order (AFO), respectively. The approach allows us to consider different in-plane magnetic fields [Figs. 1(d) and 1(f)]. In the model, we introduce the parameter l_c (coherence length). It measures the cutoff length of the dynamic dipole interaction between wires in x direction; i.e., the stray field of surrounding wires is weighted by a factor of $\exp(-x/l_c)$ [22].

In Fig. 2, we show $\Delta T(f)$ obtained with different magnetic field histories before detecting excitations (dark color). For clarity, we discuss the mode $n = 0$.

I. Saturated state with FMO.—Parallel ordering of magnetization $\mathbf{M}$ in all wires is achieved by applying a large field ($\mu_0 H_1 = +50$ mT) parallel to the wires before ramping down to a value of H at which spectra $\Delta T(f)$ are taken [cf. Fig. 2(a) to 2(c)]. A prominent magnon mode $n = 0$ is seen for fields larger than $\mu_0 H_{\mathrm{sw},1} = -14$ mT and smaller than -23 mT. Note that the resonance is not the resonance of an individual nanowire but the collective excitation of the MC [14]. Two modes appear in the field regime between -14 and -23 mT. This regime is known from bistable wires in an opposing field H [14,15]: for negative fields, $\mathbf{M}$ and $\mathbf{H}$ are antiparallel, which results in the magnetization reversal of individual wires and thereby two different magnon modes. The finite field regime reflects the distribution of the switching fields of the nominally identical wires.

II. Multidomain state.—In the following, we discuss the data shown in Figs. 2(d) and 2(e), which have been obtained in a minor loop and after microwave irradiation [14].
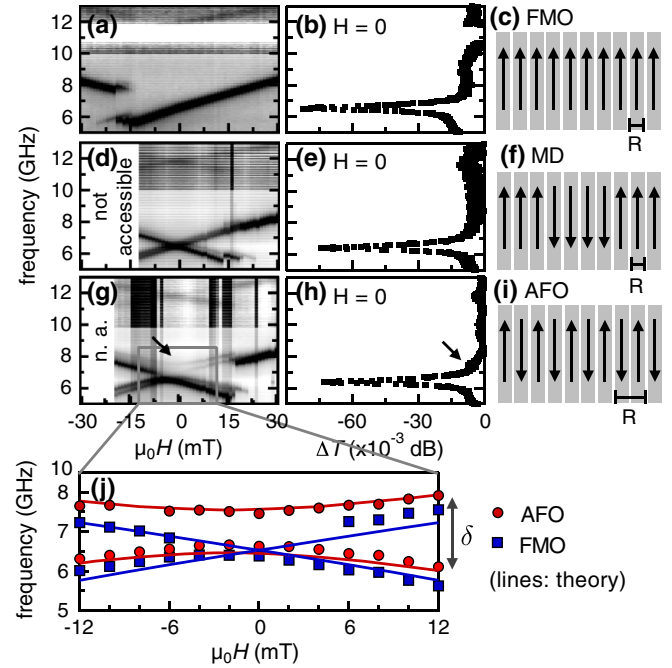

FIG. 2 (color online). Data $\Delta T(f)$ of the MC in three different magnetic states: (a) saturated state with FMO; (d) multidomain state with domains of parallel magnetization; (g) demagnetized state where parts of the MC exhibit AFO around $H = 0$. For each state, the corresponding spectrum at $H = 0$ is displayed in (b), (e), and (h), respectively. In (c), (f), and (i) the relevant configurations are sketched. (j) Resonance positions extracted from (g) and compared to theoretical predictions for MCs with FMO and AFO. The lines are shifted by -2 mT as observed for the experimental data. δ denotes the frequency separation for AFO modes. Arrows in (g) and (h) highlight the optical mode. We increased the contrast in (a), (d), and (g) for $f > 10$ GHz. The white region in (a) and black vertical stripes in (d) and (g) are artifacts due to the CPW.

Here, the MC is first saturated at $+50$ mT. Then a field of -12 mT $> \mu_0 H_{\mathrm{sw},1}$ is applied; i.e., $\mathbf{M}$ of the nanowires is antiparallel to $\mathbf{H}$. At this field, we irradiate the MC with a high-power microwave field for 1.3 s (parameters are $f = 5.3$ GHz and power $P = 16.5$ dBm). The microwave irradiation provokes microwave-assisted switching (MAS) [23,24] on selected nanowires, aligning their $\mathbf{M}$ parallel to $\mathbf{H}$. The MAS process has been investigated in detail on the same sample in Ref. [14]. The efficiency of the switching process scales with the local amplitude of h, which is largest underneath the inner conductor of the CPW and rapidly falls off in the gaps. By this means, we intended to generate domains of nanowires which have reversed while others remain in the initial state [Fig. 2(f)]. The spectra taken at fields larger than -12 mT in Fig. 2(d) now show two prominent modes in the field range between -12 and $+18$ mT. The branches cross at -2 mT [25]. This type of crossing is similar to the one shown in Fig. 1(d) where it is formed by a full and broken line. Each of these two branches represents a magnonic crystal whose magnetization is saturated fully in the $+y$ or $-y$ direction. In our

experimental data, the branch starting at low frequency at −12 mT stems from domains where neighboring wires are still magnetized in the initial direction. The branch starting at high f at −12 mT results from that part of the array where MAS successfully induced a magnetization reversal. We therefore call this particular state of the MC the multi-domain (MD) state.

III. Demagnetized state with AFO.—The third and most interesting state has been prepared by precisely adjusting a minor-loop measurement. Here, we first saturate the crystal at +50 mT and then ramp down to −19.5 mT. This value is at the center of the field regime covered by the switching field distribution. At this field, we expect that about half of the wires have been switched, thereby reaching a demag-netized state. Starting from here, we increase H again and perform a minor-loop measurement, where in remanence the demagnetized state is preserved. This state is different from scenarios I and II. In Fig. 2(h), we now observe a more complex mode pattern: modes of different intensity and, in particular, a mode repulsion near $H = 0$. Beyond +15 mT, we observe a switching process which restores the saturated state in the MC. In Fig. 2(j), we summarize the spectra around $H = 0$ by extracting the resonance positions from Fig. 2(g) and mark them with specific symbols. As lines, we draw calculated field dependencies [like in Figs. 1(d) and 1(f)] reflecting MCs with FMO and AFO. From the circular symbols, we conclude that in this minor-loop data we have generated an antiferromagnetic order. We emphasize that the mode repulsion is the experi-mental evidence of dynamic dipole interaction leading to the formation of the collective AC modes. The resonances marked by the squared symbols indicate that still parts of the MC show FMO. The reason for this intermixing lies in the statistical nature of the switching and the switching field distribution [26]. The coherence length l_c is 2.4 μm, as extracted from the comparison of the experimental data with the theory.

Microscopic analysis.—In the following, we discuss the different modes and signal strengths observed in Fig. 2. Assuming FMO, the (calculated) mode profile $m'_x(x)$ of the nth branch is a standing wave [27] with n nodes across the width of the wire inside the unit cell ($n = 0, 1, \dots$) [Fig. 3(a), left]. In our experiment, only even-numbered branches are excited and detected due to symmetry con-siderations. The $n = 0$ mode corresponds to the in-phase oscillation of m'_x in all wires. In AFO, each branch splits into two because of a new and reduced BZ [compare Figs. 1(c) and 1(e)]. R has become $2a$ [Fig. 2(i)]. The basis of the AC is composed of a pair of wires with antiparallel **M** such that the phase between the precessional motion of $m'_x(x, z)$ in both wires is relevant. The branch $n = 0$ ex-hibiting the lowest frequency has the same dispersion as the fundamental mode for the FMO state. Consequently, the mode profile is characterized by the in-phase oscilla-tion of m'_x in all wires [lower curve in Fig. 3(a), right]. Based on this it may be termed an acoustic mode. The mode of $n = 0$ with the higher frequency at $k = 0$ is
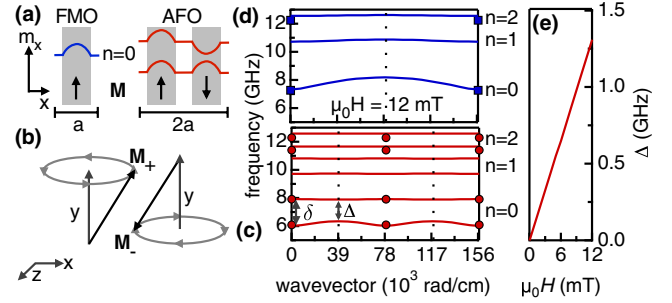

FIG. 3 (color online). (a) Schematic mode profiles m'_x vs x of branches $n = 0$ in FMO (left) and AFO (right). For clarity, we disregard here the boundary conditions leading to a finite but small amplitude at the edges [27]. (b) Precession of the optical mode based on antiparallel **M**: x (z) components move out of (in) phase, (for the acoustic mode it is vice versa) [29]. Calculated dispersions at 12 mT for (c) AFO and (d) FMO (symbols denote experimental data). Δ (δ) is defined at $k = \pi/(2a)$ ($k = 0$). (e) Calculated gap Δ for $n = 0$ of AFO.

characterized by the out-of-phase oscillation of m'_x [upper curve in Fig. 3(a), right] and thus represents an optical mode. At $k = 0$, this may be thought as originating from the boundary of the first BZ of the FMO state at $k_x = \pi/a$. Here, in the FMO state m_x in neighboring wires precesses 180° out-of-phase because $m_x(x + a) = m'_x(x)e^{i\pi}$ holds. Magnetically induced zone folding generates $k = \pi/a - G = \pi/a - 2\pi/(2a) = 0$.

The precessional motion of M is elliptical and in oppos-ing senses in neighboring wires if AFO is considered [cf. Figure 3(b)]. This implies that for an in-phase motion of m'_x in neighboring wires, the oscillation of the m'_z components is out-of-phase and vice versa. Using the quasi-1D theory of Ref. [13], we evaluate an ellipticity of $\epsilon = m'_x/m'_z = 3.6$ for $H = 0$. From this we find that the m'_x component is dominant and determines the energy of the AC modes as well as their dispersion. Excitation of the acoustic mode is pronounced via coupling of the rf field **h** to the large m'_x component of the dynamic magnetization. Instead, the m'_z component is weak. But it is still large enough such that **h** excites the optical mode where the m'_z components are found to be all in-phase in the wires [Fig. 3(b)]. The ellipticity explains the small signal strength of the upper branch for $n = 0$ in Fig. 2(g).

At $H = 0$ the Zeeman energy $E_Z = -\mu_0 M \cdot H$ is zero and the dynamic dipole interaction energy determines the mode frequencies. Quantitative comparison of the lowest dispersion branch in Fig. 1(c) with the lowest branch with the same curvature in Fig. 1(e) reveals that the curves practically coincide up to $k = \pi/(2a)$. The overall discrep-ancy is below 200 MHz since $m'_x = 3.6m'_z$ is dominant (see above). Thus, zone folding of FMO dispersions already provides a good approximation and understanding of AFO dispersions. The frequency gap Δ at the BZ boundary is zero in Fig. 1(e) because $E_Z = 0$. A periodic potential does not exist which could split the allowed bands at $k = \pi/(2a)$.

Strikingly, a gap opens at the BZ boundary for $\mathbf{H} \neq 0$ [Fig. 3(c)]. This is connected with different Zeeman energies E_Z for the wires with different orientations of $\mathbf{M}$. For the AFO state, E_Z is a periodic function of x with a period of $2a = R$. This corresponds to a periodic potential, which is tuned via H and provokes an externally controlled Bragg reflection of propagating waves. This effect has not yet been reported in earlier works considering 1D MCs [5–10,21,28]. In our AC, a forbidden frequency gap opens. For $n = 0$, Δ is found to increase up to 1.3 GHz at 12 mT [Fig. 3(e)], i.e., in the minor-loop regime addressed by the experiment. The AFO state thus results in a tunable stop band. In Fig. 3(c), every second branch decreases in frequency if compared to Fig. 1(e) where $H = 0$. The experimental data (circular symbols) in Fig. 2(j) directly substantiate the field-induced gradual down- and up-shifts of the acoustic and optical modes of the AC, respectively. These opposing shifts generate the observed mode repulsion, i.e., the variation of δ with H. Note that in Fig. 3(d), which is based on FMO, all the branches are up-shifted in frequency at 12 mT if compared to Fig. 1(c).

Best quantitative agreement between theory and data is achieved for a coherence length $l_c = 2.4$ μm (Figs. 1–3). Setting l_c to infinity, i.e., assuming long range dipolar coupling between all the nanowires, produces eigenfrequencies, which are about 1 GHz higher than depicted in Fig. 2(j) but still generates the characteristic mode repulsion. Micromagnetic simulations of the ideal nanowire array (not shown) provide, both, the mode repulsion and almost the same eigenfrequencies as our theory with $l_c = \infty$. Also, the relative mode intensities are rebuilt, which we have found in the experiment in Fig. 2(g). This means that the coherence length l_c is essential to provide, in particular, quantitative agreement concerning eigenfrequency values. It may account for unavoidable imperfections of geometric parameters of the real nanowires, i.e., rounded wire edges, edge roughness, slight deviations from array periodicity, etc. Such imperfections reduce the collective dipole field of the array. To model this, we use the factor $\exp(-x/l_c)$ to weight the contributions from neighbors of different order to the local collective dipole field [22].

In conclusion, using dense magnetic nanowire arrays we have modified the band structure of a 1D AC in a reversible manner. By selectively inducing FMO or AFO, we control the basis of the AC and the size of the Brillouin zone. For AFO, the field H switches on a periodic potential for Bragg reflection of spin waves. The reversible control of stop bands opens further pathways for research on wave phenomena in artificial crystals.

*grundler@ph.tum.de
[1] L. Esaki and R. Tsu, IBM J. Res. Dev. **14**, 61 (1970).
[2] C. Colvard et al., Phys. Rev. Lett. **45**, 298 (1980).
[3] U. Mackens et al., Phys. Rev. Lett. **53**, 1485 (1984).
[4] E. Yablonovitch, Phys. Rev. Lett. **58**, 2059 (1987).
[5] G. Gubbiotti et al., Phys. Rev. B **72**, 224413 (2005).
[6] G. Gubbiotti et al., Appl. Phys. Lett. **90**, 092503 (2007).
[7] Z. K. Wang et al., Appl. Phys. Lett. **94**, 083112 (2009).
[8] S. Nikitov, P. Tailhades, and C. Tsai, J. Magn. Magn. Mater. **236**, 320 (2001).
[9] V. Kruglyak and R. Hicken, J. Magn. Magn. Mater. **306**, 191 (2006).
[10] K.-S. Lee, D.-S. Han, and S.-K. Kim, Phys. Rev. Lett. **102**, 127202 (2009); S.-K. Kim, K.-S. Lee, and D.-S. Han, Appl. Phys. Lett. **95**, 082507 (2009).
[11] S. Neusser and D. Grundler, Adv. Mater. **21**, 2927 (2009).
[12] V. V. Kruglyak et al., Phys. Rev. Lett. **104**, 027201 (2010).
[13] M. P. Kostylev, A. Stashkevich, and N. Sergeeva, Phys. Rev. B **69**, 064408 (2004).
[14] J. Topp, D. Heitmann, and D. Grundler, Phys. Rev. B **80**, 174421 (2009).
[15] J. Jorzick et al., Phys. Rev. B **60**, 15194 (1999).
[16] F. Giesen, J. Podbielski, and D. Grundler, Phys. Rev. B **76**, 014431 (2007).
[17] S. Kalarickal, P. Krivosik, M. Wu, and C. E. Patton, J. Appl. Phys. **99**, 093909 (2006).
[18] T. J. Silva, C. S. Lee, T. M. Crawford, and C. T. Rogers, J. Appl. Phys. **85**, 7849 (1999).
[19] G. Counil et al., J. Appl. Phys. **95**, 5646 (2004).
[20] K. J. Kennewell, M. Kostylev, and R. L. Stamps, J. Appl. Phys. **101**, 09D107 (2007).
[21] M. Kostylev et al., Appl. Phys. Lett. **92**, 132504 (2008).
[22] G. Gubbiotti et al., arXiv:1004.1881 [J. Phys. D (to be published)].
[23] J. Podbielski, D. Heitmann, and D. Grundler, Phys. Rev. Lett. **99**, 207202 (2007).
[24] G. Woltersdorf and C. H. Back, Phys. Rev. Lett. **99**, 227207 (2007).
[25] Most likely, the individual domains in the MD state cover different areas and produce a residual stray field component of -2 mT, self-biasing the wires tested by the CPW.
[26] The mode repulsion behavior was verified on an array with AFO where every second nanowire exhibited a slightly different width. l_c amounted to 2.7 μm.
[27] K. Y. Guslienko, S. O. Demokritov, B. Hillebrands, and A. N. Slavin, Phys. Rev. B **66**, 132402 (2002).
[28] A. V. Chumak et al., J. Appl. Phys. **105**, 083906 (2009).
[29] The effective field H_{eff} of neighboring wires is in y direction and antiparallel for AFO by definition. Using the Landau-Lifshitz equation $\partial \mathbf{M}/\partial t \propto -\mathbf{M} \times \mathbf{H}_{\mathrm{eff}}$ provides the precessional motion as sketched.